Proceedings of the 2001 IEEE
International Conference on Robotics & Automation
Seoul, Korea · May 21-26, 2001

Path Planning for Robot-Assisted Grinding Processes

Y.T. Wang and Y.J. Jan
Department of Mechanical Engineering, Tamkang University
151 Ying-Chuan Rd., Tamsui, Taipei, Taiwan 25137
ytwang@mail.tku.edu.tw

Abstract

Path planning for a robot-assisted surface finishing system with an active torque controller is presented in this paper. We utilize a dexterous manipulator to attain the desired position and orientation in three-dimensional space during finishing processes. A single-axis active controller consists of a dc motor and a software observer is attached to the robot wrist and used to actuate a pneumatic hand-grinder. The torque observer is designed to sense the grinding contact force based on the driving current and output position of the motor. Zigzag and fractal paths on curved surfaces are designed for the grinding processes. In order to determine an ideal grinding condition, Taguchi's method for experimental design is utilized. We choose four grinding conditions, namely, path pattern, grinding contact pressure, tool diameter, and feed rate. Tendencies of these factors can be found from the experiments. In this research, the prototype of a robot-assisted finishing system is constructed and tested on a Tatung A530 robot. The experimental results show that the robot-assisted finishing system functions well under a variety of grinding conditions.

1. Introduction

Finishing processes of die-cast manufacturing include grinding, honing, lapping, polishing lapping, and polishing. These processes are time-consuming and monotonous operations that strongly rely on skilled human-workers. To automate these processes and achieve desired surface roughness, it is important to control the grinding path and contact force, as well as to choose suitable feed-rate and tool diameter. Among them, to generate a suitable tool-path and to control the contact force are two major challenge issues. For example, to polish free-form surfaces of an object requires a delicate machine to follow complicated polishing paths. In this case, a polishing system based on a robot manipulator is more effective than that on a NC machining center in order to follow the curved free-form surfaces. Different robot grinding path on the specimen will affect the surface roughness. On the other hand, during finishing operations, the tool comes into physical contact with the workpiece and causes contact forces between them. It is difficult to control these contact forces which depend on the cutting depth, feed rate, grinding-wheel speed and material properties.

Many researchers have proposed automated systems for grinding of dies, deburring of castings, and removing of weld beans etc [5-8]. Usually, a grinding tool is mounted on a NC machining center or a robot manipulator and a multi-dimensional force sensor is included in the system to improve finishing accuracy. It is troublesome to handle the multi-dimensional motion and force control system in run-time processes, besides the passive-type force sensors are expensive in price and sensitive to a noise.

We propose an automated finishing system for polishing free-form surfaces of dies specimens. Two types of tool path, zigzag and fractal, are used in this research for comparison. To simplify the force-control action, only the contact force normal to the polishing surface is concerned and a software-type torque observer is used to replace the role of a hardware sensor. We decide four important grinding conditions, namely, path pattern, grinding contact pressure, tool diameter, and feed rate. In order to determine the best combination of the four grinding conditions, Taguchi's method for experimental design is utilized.

2. Finishing robot system

The developed robot-assisted surface finishing system consists of a 5-axis articulated industrial robot, an end-effector, a robot controller, a xy-table for setting the metal mold, and a personal computer for sensory processing essential to a contact force control. The system configuration is shown as Figure 1. The system utilizes a dexterous manipulator, Tatung A530, to attain the desired position and orientation of the end-effector in three-dimensional space. A dc motor is attached to the robot wrist and used to actuate the polishing tool. The torque observer is designed to sense the applied torque based on the driving current and output position of the dc motor. A pneumatic hand-grinder is serially mounted on the observer-motor. We control the motion and contact force of the hand-grinder to perform the desired finishing action. The robot follows a desired tool path and drives the hand-grinder to come in contact with the workpiece. The single-axis torque observer can sense the contact force and direct the hand-grinder to apply a desired contact pressure

on the workpiece. The kinematic analysis, path planning, and torque control algorithm for the robot and torque observer are derived in the following sections.

In order to polish a workpiece with free-form surfaces, a 7-d.o.f. mobility is provided by the finishing system formed by a Tatung A530 robot and a xy-table as shown in Figure 1. The workpiece is placed on the xy-table. During the process, the manipulator drives the polishing tool to follow a programmed path and attain a desired orientation. The robot performs rotation in three rotational angles and translation in z-axis, while the xy-table translates in x- and x-axis. There is one more d.o.f. mobility provided by the dc observer-motor. We control the current command and the angular position of the motor in order to ensure that the tool is kept at a desired contact angle and contact pressure with the workpiece. Usually, the contact angle, θ_f, is measured from the surface at contact point in the drive-feed direction as shown in Figure 2.

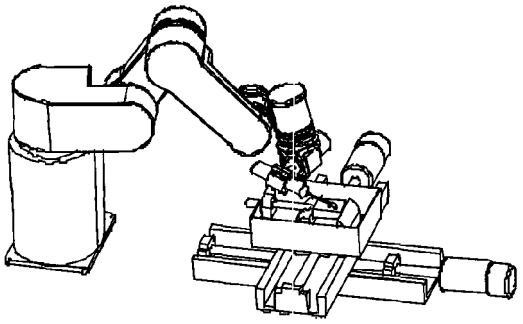

Figure 1 Finishing Robot System

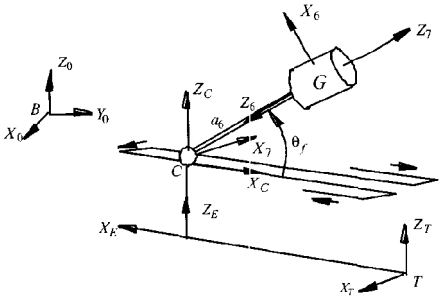

Figure 2 Coordinate systems for the contact area

Assume that the contact angle is retained at a magnitude of θ_f, and the contact at point C is a point contact, then the homogenous transformation matrix from the robot-base coordinate, B, to the coordinate of the contact point, C, can be expressed as

$$A_C^B = A_T^B A_C^T = A_P^B A_C^P$$

where T and P are located at the coordinate origins of the base of the xy-table and the robot end-effector, respectively. During the finishing process, the desired position coordinate of the contact point C and the orientation of the tool relative to surfaces of the specimen are generated. The transformation from the robot-base frame to the end-effector is determined by

$$A_P^B = A_T^B A_C^T (A_C^P)^{-1} = A_C^B (A_C^P)^{-1} \quad (1)$$

where A_C^P could be found by the knowledge of θ_f and tool length. From Equation (1), we can find the desired joint angles of A530 robot by an inverse kinematic method. These joint angles are the inputs of the robot motion controller.

3. Grinding Path Planning

We use B-spline function to describe the surface of a specimen,

$$Q(u,v) = \sum_{i=1}^{n+1} \sum_{j=1}^{m+1} B_{i,j} N_{i,k}(u) M_{j,l}(v)$$

Where $B_{i,j}$ is a position matrix; $N_{i,k}(u)$ and $M_{j,l}(v)$ are two basis functions in u and v axes respectively. Typical curved surfaces of a specimen are shown in Figures 3 and 4. We can formulate different types of tool path for the robot to perform a task on this workpiece. Two types of tool path, zigzag and fractal, are used in this research for comparison. A zigzag is a path with repeated switching of directions as shown in Figure 3. Figure 5 depicts the top-view of a specimen ground by zigzag tool path. On the other hand, a fractal tool path is generated based on the Hilbert "£v" pattern. A L-system method [4] using logical symbols is adopted here to generate the Hilbert "£v" pattern. Definitions of the logical symbols are stated as following:

F: *Drawing a fixed-length line from current position to new position*
-: *Turning an angle of 90° in CCW direction*
+: *Turning an angle of 90° in clockwise direction*
L: +F-F-F+
R: -F+F+F-

Generation rules of the Hilbert curve are: (a) substituting "+RF-LFL-FR+" into L, "-LF+RFR+FL-" into R when the order increases by one, (b) repeating the processes in every increment of order, and (c) the zero-order starting from the L-operation.

Figure 4 depicts a 3rd-order fractal tool path based on the generation rules, while the top-view of the ground specimens by fractal tool path are shown in Figure 5-7. We found that the fractal path has an advantage of consistency in direction [4].

We develop a PID position controller for the motion of each axis of the xy-table. The control block diagram is shown in Figure 8 and the transfer function is given by

$$\frac{P(s)}{P^*(s)} = \frac{K_t K_d s^2 + K_t K_p s + K_t K_i}{Js^3 + (B + K_t K_d)s^2 + K_t K_p s + K_t K_i}$$

Where $P^*(s)$ and $P(s)$ represent the position command and output, respectively; J is the inertia and B is the coefficient

of viscous friction; K_t is the drive torque constant; K_p, K_i, K_d are gains of the PID controller. For the xy-table, point-to-point motion is programmed by using a trapezoid velocity profile as shown in Figure 9.

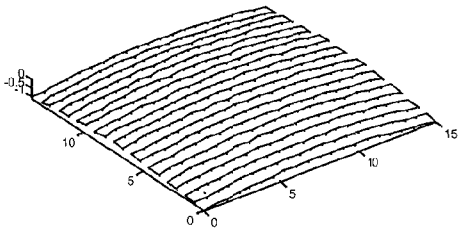

Figure 3 Zigzag tool path

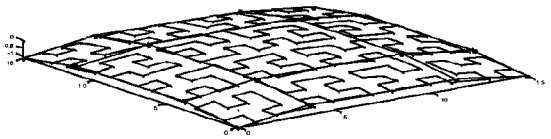

Figure 4 Third-order fractal tool path

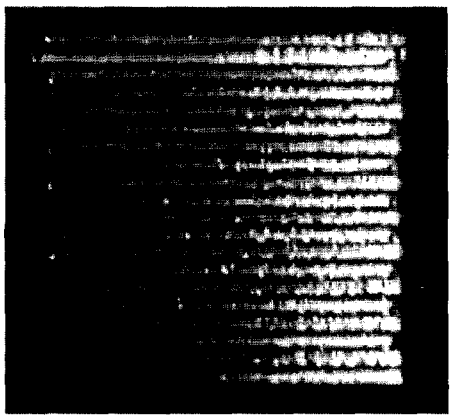

Figure 5 Ground zigzag tool path

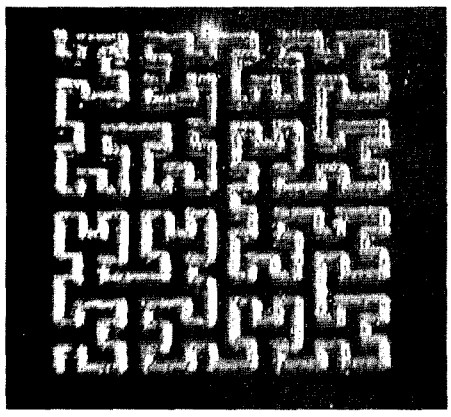

Figure 6 Ground 3rd-order fractal path

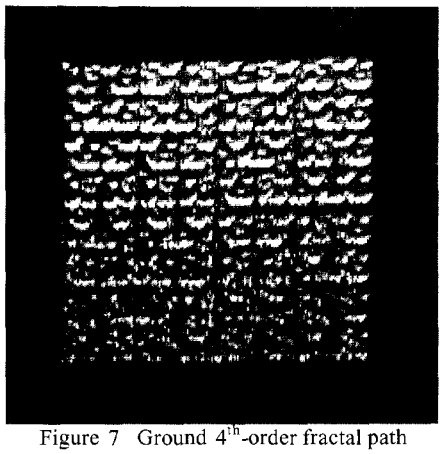

Figure 7 Ground 4th-order fractal path

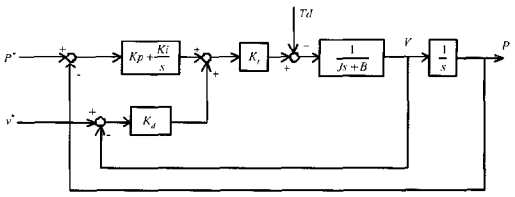

Figure 8 PID position control

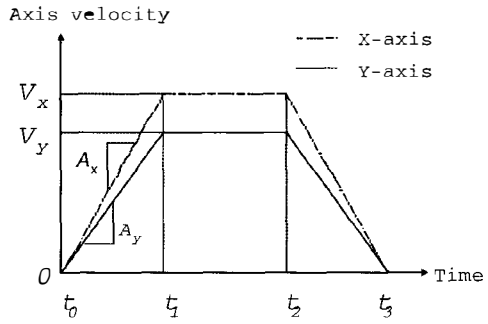

Figure 9 Trapezoid velocity profile

4. Contact torque control

In the finishing process, an incorrect CAD data or tool wear will cause a contour error. In this case, a pure position controller would cause the tool to be no contact with or over-cut the workpiece. A suitable torque controller is always needed in a finishing process. In this research, we propose to control only the contact pressure normal to the contact surface. Then the torque controller could be simplified and decoupled from the robot motion controller.

We model the contact behavior between the tool and the specimen as a linear rotational spring in Figure 10,

$$T_f = k_e \theta \tag{2}$$

where T_f is the torque exerted by the observer motor on the surface of the workpiece; k_e is the rotational spring

constant; θ is the angular displacement of the motor. The dynamic equation of the end-effector system with an observer motor and a hand-grinder can be expressed as

$$T_{em} = J\ddot{\theta} + k_e\theta + T_L \qquad (3)$$

where T_{em} and T_L are the applied torque and external load, respectively. J is the inertia of the system. From Equation (2), we have

$$\theta = k_e^{-1}T_f$$
$$\ddot{\theta} = k_e^{-1}\ddot{T}_f$$

Equation (3) can be rewritten as the following equation with the new variable T_f,

$$T_{em} = Jk_e^{-1}\ddot{T}_f + T_f + T_L \qquad (4)$$

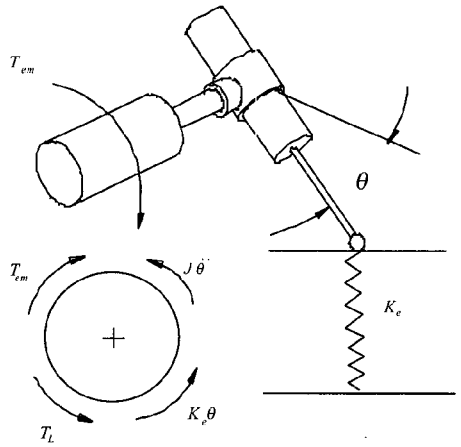

Figure 10 Linear spring model

In order to control the applied torque, a proportional-integral-derivative (PID) controller is considered

$$T_{em} = Jk_e^{-1}\left[\ddot{T}^* + k_{fp}e_f + k_{fi}\int e_f dt + k_{fd}\dot{e}_f\right] + T_f + T_L \qquad (5)$$

where T^* denotes the torque command; e_f is the torque error, $e_f = T^* - T_f$; k_{fp}, k_{fi} and k_{fd} are the gain values of the PID controller. In this case, T_L is not suitable to be put in the controller because it is not easy to be measured on-line. The term $(T_f + T_L)$ in Equation (5) is replaced by a feed-forward command T^*. The resultant controller is a PID-plus-feedforward (PIDFF) controller,

$$T_{em} = Jk_e^{-1}\left[\ddot{T}^* + k_{fp}e_f + k_{fi}\int e_f dt + k_{fd}\dot{e}_f\right] + T^* \qquad (6)$$

The block diagram of the PIDFF controller is shown in Figure 11. Where k_t is the torque constant of the motor; $\hat{J}$, $\hat{k}_e$ and $\hat{k}_t$ are the estimated values of the system parameters J, k_e and k_t, respectively. In the feedback loop, we replace sT_f by $k_e\omega$ in order to reduce the signal noise to the controller. Where ω is the angular speed of the motor. In the finishing processes, the contact torque will be kept at a constant value, *i.e.* $\dot{T}^* = \ddot{T}^* = 0$. From Equations (4) and (6), we find the error equation,

$$\ddot{e}_f + k_{fd}\dot{e}_f + \frac{e_f}{Jk_e^{-1}} + k_{fi}\int e_f dt = T_L$$

$$\dddot{e}_f + k_{fd}\ddot{e}_f + k_{fp}\dot{e}_f + k_{fp}\dot{e}_f + k_{fi}e_f = \dot{T}_L \qquad (7)$$

We can see that he value of the steady-state error vanishes as time approaches infinity. If the estimated values of the system parameters are correct, we can derive the transfer function which represents the relationship between the output torque, T_f, and the command torque, T^*,

$$\frac{T_f}{T^*} = \frac{(Jk_{fp} + k_e)s + Jk_{fi}}{Js^3 + Jk_{fd}s^2 + (Jk_{fp} + k_e)s + Jk_{fi}} \qquad (8)$$

In the case of no disturbance, the output will track the command exactly at steady state, as we can see from Equations (7) and (8). If there exists a disturbance, T_L, the steady-state error will disappear as time approaches infinity. The PIDFF controller provides a solution to the torque control problem during the finishing process. The analytical and experimental works in this paper are based on the concept of the PIDFF controller.

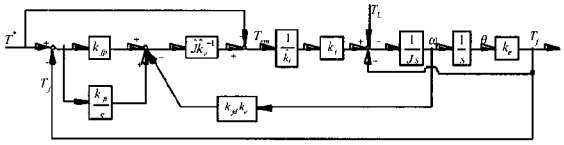

Figure 11 Block diagram of the PIDFF controller

5. Torque observer

We utilize a torque observer to estimate the contact torque during the finishing processes. The torque observer is a linear Luenberger observer [9] as shown in Figure 12. The block diagram is composed of two parts: the upper loop is the motor system with a torque controller and the lower one is the torque observer. The torque observer estimates the contact torque based on the information of the torque command and the output position of the system.

According to Figure 12, the observed torque can be determined as

$$\hat{T}_f = \frac{\frac{\hat{k}_t}{k_t}(k_{od}s^2 + k_{op}s + k_{oi})}{\hat{J}s^3 + k_{od}s^2 + k_{op}s + k_{oi}}T_f + \frac{\hat{J}(k_{od}s^3 + k_{op}s^2 + k_{oi}s)}{\hat{J}s^3 + k_{od}s^2 + k_{op}s + k_{oi}}\left[\left(\frac{J}{\hat{J}}\frac{\hat{k}_t}{k_t} - 1\right)\omega\right] \qquad (9)$$

Where k_{op}, k_{oi} and k_{od} are gains of the observer. If the parameters, $\hat{k}_t$ and $\hat{J}$, are correctly estimated, Equation (9) can be simplified as

$$\frac{\hat{T}_f}{T_f} = \frac{(k_{od}s^2 + k_{op}s + k_{oi})}{\hat{J}s^3 + k_{od}s^2 + k_{op}s + k_{oi}} \qquad (10)$$

In steady state, the torque observer can sense the contact torque exactly.

The parameters of the dc observer-motor system are listed in Table 1. The controller is equipped with a PCL-726 D/A interface card and a PCL-833 encoder card by Advantech [1,2]. The D/A card has a 12-bits resolution to represent the output current in the range of $\pm 5A$. The basic unit of the current command of the motor drive is calculated as

$$10A \times \frac{1}{2^{12}} = \frac{10}{4095} \cong 2.44\,mA$$

The resolution of the observer is

$$T = i \times k_t = 2.44\,mA \times 0.185\,\frac{N \cdot m}{Amp}$$

$$= 0.4514\,mN \cdot m \times \frac{1\,kgf}{9.81\,N} \cong 4.601 \times 10^{-2}\ kgf \cdot mm$$

The radius between the motor axis and the contact point is $95\,mm$. Then, the resolution of the applied pressure is

$$4.601 \times 10^{-2} / 95\ mm = 0.48\ gf$$

This is the smallest force can be applied by the active torque controller. On the other hand, the maximum output-torque is limited by the rate-current of the motor which value is 1 amp ere in this case. The maximum output torque can be generated by the controller is determined as

$$T = 0.185\frac{N \cdot m}{Amp} \times 1\,Amp \times \frac{1\,kgf}{9.81\,N} \times \frac{1000mm}{1m} \cong 18.9\ kgf \cdot mm$$

which is about 199 gf for this system.

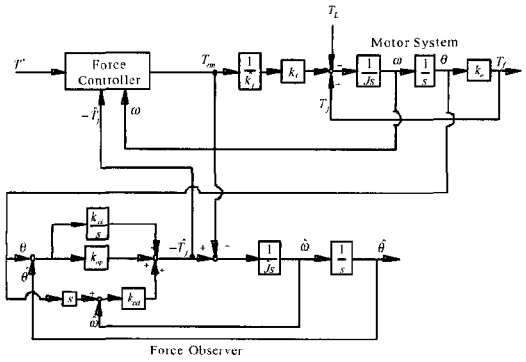

Figure 12 Torque controller with a Luenberger observer

Table 1 Parameters of the observer-motor

Rated Power	*60Watt*
Rated Voltage	*75V*
Rated Current	*1.2A*
Torque Constant	*0.185N·m/A*
Rotor Inertia	*1.72656×10⁻⁵kg·m²*
Weight	*0.8kgf*

6. Taguchi's Parametric Design

The integrated robot-assisted finishing system is shown in Figure 13. The system includes a Tatung A530 robot for implementing the position and orientation of finishing processes. The torque observer is a 60*watt* dc motor which is serial-connected to the wrist of the robot. The pneumatic hand-grinder is equipped at the front end of the torque observer. The motion of the manipulator is controlled by a single-board controller. The estimated inertia and contact stiffness of the hand-grinder system are

$$\hat{J} \cong 0.0011\ kgm^2$$

$$\hat{k}_e = 11.95\ Nm/rad$$

The gains of the controller and observer are given as

$$k_{fp} = 299.3636;\quad k_{fi} = 226981;\quad k_{fd} = 183$$

$$k_{op} = 5.28;\quad k_{oi} = 70.4;\quad k_{od} = 0.132$$

The purpose of Taguchi's parametric design is to determine the best programming of the four grinding factors, namely, tool diameter, path pattern, federate, and grinding contact pressure. In this paper, Taguchi's L_{18} orthogonal table is used as shown in Table 2. Taguchi's L_{18} table has the property that interactions are distributed uniformly among all factors and the major trend of each factor can still be seen.

Experimental results are expressed in terms of the signal to noise ratio (or S/N ratio) η, which is defined by the decibel value of surface roughness R_a,

$$\eta = -10\log(R_a)^2 = -20\log(R_a)$$

The surface roughness R_a is defined by the arithmetic mean values of surface heights

$$R_a = \frac{a+b+c+d+\ldots}{n}$$

where $a, b, c, d, \ldots$ are absolute values of surface heights measured in μm.

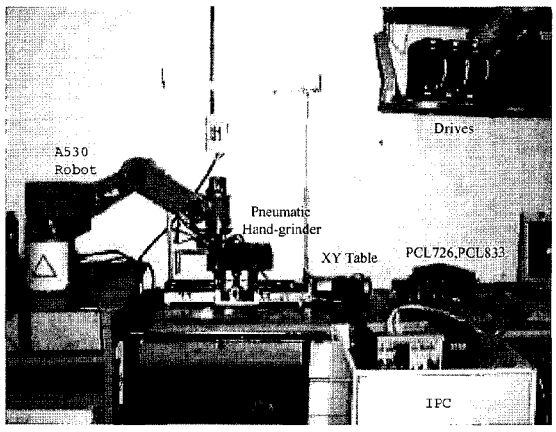

Figure 13 Automated Surface Finishing System

In this experiment, we have four grinding factors with several levels shown as follows,

Tool Diameter	3mm, 4mm
Path Pattern	zigzag(200μm), 5th-order fractal, 4th-order Fractal
Feedrate	12.5mm/s, 25mm/s, 37.5mm/s
Grinding Pressure	0.556N, 1.111N, 1.667N

Note that, only the scale of tool diameter is divided into two levels, scale of all the other factors are divided into three levels. Results for the various factors are also shown in the last two columns of Table 2. According to the method in reference [3], contribution of each factor is calculated, and the results are shown in Table 3. From this table, we know that among the four factor which may affect surface roughness, their contribution in descending order are path pattern, grinding contact pressure, tool diameter, and feed rate. The signal-to-noise ratio for each of the grinding factors can be determined from Table 2. The results show that the best combination of the grinding factors is $A_1B_1C_1D_3$, which includes 4-mm tool diameter, 5th-order fractal path, 12.5mm/s federate, and 1.667N grinding pressure.

Table 2 Experiment design and results

	tool diameter (mm)	path pattern	feed-rate (mm/sec)	grinding pressure (N)	Surface roughness Ra(μm)	SN Ratio η_i
1	4	5th-order fractal	12.5	0.556	5.000	6.021
2	4	5th-order fractal	25	1.111	3.500	9.119
3	4	5th-order fractal	37.5	1.667	3.750	8.519
4	4	4th-order fractal	12.5	0.556	8.250	1.671
5	4	4th-order fractal	25	1.111	6.000	4.437
6	4	4th-order fractal	37.5	1.667	6.000	4.437
7	4	zigzag	12.5	1.111	4.250	7.432
8	4	zigzag	25	1.667	5.250	5.597
9	4	zigzag	37.5	0.556	6.750	3.414
10	3	5th-order fractal	12.5	1.667	4.500	6.936
11	3	5th-order fractal	25	0.556	6.250	4.082
12	3	5th-order fractal	37.5	1.111	5.000	6.021
13	3	4th-order fractal	12.5	1.111	7.500	2.499
14	3	4th-order fractal	25	1.667	6.750	3.414
15	3	4th-order fractal	37.5	0.556	10.500	-0.424
16	3	zigzag	12.5	1.667	6.750	3.414
17	3	zigzag	25	0.556	9.250	0.677
18	3	zigzag	37.5	1.111	6.500	3.742

Table 3 Contribution of various factors

Factors	Degree of freedom (DF)	Sum of squares (SS)	Variance (V)	Pure sum of squares (TS)	Percent contribution (%)
Tool diameter	1	22.862	22.862	22.862	20.2%
Path pattern	2	52.549	26.275	52.549	46.5%
Federate	2	0.453	0.227	0.453	0.4%
Grinding pressure	2	33.487	16.744	33.487	29.6%
Error		3.656			3.3%
sum	7	113.008			100.0%

7. Conclusions

This paper presents the development of a robot-assisted surface finishing system with an active torque controller. This system utilizes a dexterous manipulator to attain the desired position and orientation of finishing processes in three-dimensional space. A torque observer is attached to the tool frame of the robot manipulator, and a pneumatic hand-grinder is serially mounted on the observer. The function of the active torque controller in the system includes observing the contact torque, applying a desired contact pressure in the normal direction of the workpiece surface, and adjusting the contact angle between the hand-grinder and the surface of the workpiece. In this research, we construct the prototype of a robot-assisted finishing system. The experimental results show that the developed torque observer and controller system functions well under a variety of grinding conditions.

Taguchi's method is used to determine the effects of the following factors: tool diameter, path pattern, federate, and grinding contact pressure. Tendencies of these factors are found. From the experimental results, we know that among the four factor which may affect surface roughness, their contribution in descending order are path pattern, grinding contact pressure, tool diameter, and feed rate.

Acknowledgement

This work was supported by the National Science Council in Taiwan under grant no. NSC89-2212-E-032-008.

References

[1] Advantech, 1994a, PCL-726 six-channel D/A output card user's manual.

[2] Advantech, 1994b, PCL-833 3-axis quadrature encoder and counter card user's manual.

[3] Belavendram, N., Quality by Design, Prentice Hall, 1995.

[4] Chen, A.C.-C., K.C. Tai, C.H. Chen, Y.C. Wang, P.H. Lo, and Y.T. Wang, 1998, Generation of Fractal Tool Paths for Automated Surface Finishing Processes, Pacific Conference on Manufacturing, Brisbane, Australia.

[5] Furukawa, T., D.C. Rye, M.W.M.G. Dissanayake, and A.J. Barratt, 1996, Automated polishing of an unknown three-dimensional surface, Robotics & Computer-Integrated Manufacturing, Vol.12, No.3, pp.261-270.

[6] Jenkins, H.E. and T.R. Kurfess, 1996, Design of A Robust Controller for A Grinding System, IEEE Transactions on Control Systems Technology, Vol. 4, No.1, pp.40-48.

[7] Kunieda, M., T. Nakagawa, and T. Higuchi, 1984, Development of a Polishing Robot for Free Form Surface, Proceedings of the 5th International Conference on Production Engineering, pp.265-270, Tokyo.

[8] Kurfess, T.R., D.E. Whitney, and M.L. Brown, 1988, Verification of a dynamic grinding model, Journal of Dynamic systems, Measurement and Control, Vol.110, n4, pp.403-409.

[9] Luenberger, D.G., 1971, An Introduction to Observers, IEEE Transactions on automatic control, Vol. AC-16, No. 6, pp.596-602.

[10] Perdikaris, G.A. and K.V. VanPatten, 1982, Computer Schemes for Modeling, Tuning, and Control of DC Motor Drive Systems, Proceedings of the Power Electronics International Conference, pp.83-96.